Research Square

Preprints are preliminary reports that have not undergone peer review.
They should not be considered conclusive, used to inform clinical practice,
or referenced by the media as validated information.

# Drp1-Associated Mitochondrial Dysfunction Is Involved in PNA-TPP-Mediated Reduction of Cisplatin Tolerance in A549 Lung Adenocarcinoma Stem-like Spheres

**lixia xie**
The Second Affiliated Hospital of Nanchang University, Jiangxi Medical College, Nanchang University
**yong cheng**
The Second Affiliated Hospital of Nanchang University, Jiangxi Medical College, Nanchang University
**guofeng zhu**
The Second Affiliated Hospital of Nanchang University, Jiangxi Medical College, Nanchang University
**xinyi zhang**
The Second Affiliated Hospital of Nanchang University, Jiangxi Medical College, Nanchang University
**xiaoqun ye**
511201663@qq.com

The Second Affiliated Hospital of Nanchang University, Jiangxi Medical College, Nanchang University

**Research Article**

**Keywords:** PNA-TPP, Drp1, mitochondrial dysfunction, cisplatin tolerance, lung adenocarcinoma

**Posted Date:** July 6th, 2026

**DOI:** https://doi.org/10.21203/rs.3.rs-10077419/v1

**License:** This work is licensed under a Creative Commons Attribution 4.0 International License.
Read Full License

**Additional Declarations:** No competing interests reported.

## Abstract

# Background

Cisplatin (CDDP) resistance reduces the treatment effect in non-small cell lung cancer. Lung cancer stem-like cells are closely linked to drug tolerance. Mitochondrial dysfunction may affect their stemness and response to treatment. This study examined whether peptide nucleic acid conjugated with triphenylphosphonium (PNA-TPP) could reduce cisplatin tolerance in A549 lung adenocarcinoma stem-like spheres. We also explored whether this effect was related to Drp1 (dynamin-related protein 1)-associated mitochondrial changes.

# Methods

A549-derived stem cell-like spheres were established by single-cell cloning and serum-free suspension culture. PNA-TPP was designed to target the mitochondrial DNA D-loop region and was used at 10 nmol/mL for 24 h. Cell viability, colony formation, sphere formation, apoptosis, migration, and invasion were assessed using CCK-8, colony formation, sphere formation, Annexin V-FITC/PI flow cytometry, wound healing, and Transwell assays. Mitochondrial membrane potential, reactive oxygen species (ROS), and ATP levels were detected using JC-1 staining, DCFH-DA flow cytometry combined with DHE fluorescence staining, and ELISA, respectively. Drp1 expression was examined by qRT-PCR and Western blotting. Drp1 overexpression and shRNA-mediated knockdown were used to evaluate its involvement.

# Results

PNA-TPP increased Drp1 mRNA expression and mitochondrial Drp1 levels. PNA-TPP reduced mitochondrial membrane potential and ATP levels, increased ROS levels, and decreased sphere-forming ability and octamer-binding transcription factor 4 (OCT4), SRY-box transcription factor 2 (SOX2), and Nanog homeobox (NANOG) expression. PNA-TPP pretreatment further enhanced cisplatin-induced inhibition of cell viability, colony formation, migration, and invasion, and increased apoptosis. Drp1 overexpression partly mimicked these effects, whereas Drp1 knockdown partially restored mitochondrial membrane potential and stemness-related phenotypes after PNA-TPP treatment.

# Conclusion

PNA-TPP may reduce cisplatin tolerance in A549 lung adenocarcinoma stem cell-like spheres by inducing Drp1-associated mitochondrial dysfunction and weakening stemness-related phenotypes.

## 1 Introduction

Lung cancer is still a leading malignant tumor worldwide. Non-small cell lung cancer represents the main subtype, and lung adenocarcinoma is among its most common pathological forms [1–4]. Cisplatin is an important chemotherapeutic drug for non-small cell lung cancer. However, acquired resistance can reduce its therapeutic effect and is associated with tumor recurrence and poor prognosis [5–7]. Cisplatin resistance is related not only to enhanced DNA damage repair, escape from apoptosis, and abnormal cell cycle regulation, but also to phenotypic remodeling and increased stemness of tumor cells [8–10]. Previous studies have reported that cisplatin exposure may increase the proportion of cancer stem-like cells in non-small cell lung cancer and make these cells less sensitive to different drugs [9]. In addition, cisplatin-resistant A549 cells may show metabolic changes such as increased mitochondrial mass, suggesting that mitochondrial status may be involved in the formation of the drug-resistant phenotype in lung cancer cells [11].

Mitochondria are the main sites of adenosine triphosphate (ATP) production. They also participate in ROS generation, membrane potential regulation, and intrinsic apoptosis. In lung cancer cells, mitochondrial homeostasis is closely linked to cell growth, invasion, and treatment response. For example, TIM-4 may enhance oxidative phosphorylation and mitochondrial function through the ANXA2/PI3K/AKT/OPA1 pathway. This process may promote lung cancer progression [12]. Another study showed that mitochondrial DNA mutations may be involved in cisplatin resistance in A549 cells. This result further supports the link between mitochondrial functional changes and chemotherapy response in lung cancer [13]. Therefore, disruption of mitochondrial homeostasis in lung cancer stem cell-like cells may be an effective strategy to reduce their stemness and cisplatin tolerance.

Mitochondrial dynamics play an important role in preserving mitochondrial homeostasis. The balance between mitochondrial fission and fusion can influence energy metabolism, oxidative stress, and sensitivity to apoptosis. Drp1 is a core mediator of mitochondrial fission. Although Drp1 is encoded by nuclear DNA and is mainly present in the cytoplasm, it can be recruited to mitochondria under specific conditions. Only the mitochondrial fraction of Drp1 directly participates in the fission process. In tumor cells, dysregulated Drp1-related mitochondrial dynamics may affect cell survival and the response to chemotherapy. Previous studies have reported that the mitochondrial dynamics-related p32/OPA1 axis is involved in cisplatin resistance in non-small cell lung cancer [11]. In addition, DRP1-mediated mitochondrial fission has been closely linked to apoptosis regulation and antitumor treatment response [14]. These findings suggest that regulation of Drp1-mediated mitochondrial functional changes may provide a new entry point for reversing drug resistance in lung cancer stem cell-like cells.

In our previous work, PNA-TPP was constructed by coupling a PNA sequence targeting the mitochondrial DNA D-loop regulatory region with the triphenylphosphonium cation TPP. We found that PNA-TPP promoted mitochondrial enrichment of PNA through the mitochondrial membrane potential. In addition, PNA-TPP interfered with mitochondrial-related gene expression, reduced ATP levels and mitochondrial membrane potential, and enhanced the cytotoxic effect of cisplatin on A549 tumor spheres. Based on this evidence, the present study aimed to further explore whether PNA-TPP can induce mitochondrial dysfunction associated with Drp1 changes in A549 lung adenocarcinoma stem

cell-like cells, and to examine whether this process is related to reduced stemness phenotype and enhanced cisplatin-mediated inhibition.

## 2 Materials and Methods

# 2.1 Cell culture

The A549 cell line was obtained from American Type Culture Collection (ATCC). The identity of the cell line was authenticated by the cell bank before distribution, and no additional in-house short tandem repeat (STR) authentication was performed before the experiments. Cells were routinely examined and confirmed to be free of mycoplasma contamination before use in the experiments. Cells were grown in DMEM supplemented with 10% fetal bovine serum (FBS, 10099-141, Gibco). The culture condition was 37°C with 5% $CO_2$. After recovery from frozen storage, cells were placed in 6-cm dishes. The medium was refreshed based on cell growth. Subculture was performed when cells reached about 70%–80% confluence. The cells were first rinsed with PBS. Next, 1 mL of 0.25% trypsin (T1300, Solarbio) was used for digestion. When cells rounded up and detached, digestion was terminated with the same volume of medium containing 10% FBS. The cell suspension was centrifuged at about 100 × g for 4 min. The pellet was then resuspended in 4 mL complete medium and transferred into new dishes. Cells with good growth status in the logarithmic phase were used for monoclonal culture, sphere induction, and subsequent assays.

# 2.2 Generation of A549-derived lung cancer stem-like spheres

A549 stem-like spheres were generated by serum-free suspension culture. The sphere medium contained DMEM/F12 medium (11320033, Gibco/Thermo Fisher Scientific), B27 supplement (50×, 17504044, Gibco/Thermo Fisher Scientific), epidermal growth factor (EGF) (AF-100-15, PeproTech), basic fibroblast growth factor/fibroblast growth factor 2 (bFGF/FGF-2) (100-18B, PeproTech), and insulin. Each 100 mL DMEM/F12 medium was supplemented with 2 μg EGF, 2 μg bFGF, 2 mL 50× B27, and 250–275 μL insulin. The medium was prepared under sterile conditions and kept at 4°C. Log-phase A549 cells were rinsed with PBS and digested with trypsin-EDTA. Complete medium containing 10% fetal bovine serum was used to stop digestion. The cells were then made into a single-cell suspension. Cells were plated in 6-well plates at 30–50 cells/well and maintained at 37°C with 5% $CO_2$. Fresh medium was added every 2–3 days. After 7–9 days, compact colonies derived from single cells were selected. These colonies were digested again, placed in serum-free medium, and gently pipetted 80–100 times. The cells were then transferred to low-attachment 6-well plates at about $1 \times 10^3$ cells/well. Fresh serum-free medium was added every 3–5 days. After 10–14 days, floating spheres were collected as first-generation A549 stem cell spheres. The spheres were allowed to settle for 30 min. The supernatant was removed. Fresh serum-free medium was added. The spheres were gently dissociated and cultured for another 1–2 weeks. The obtained second-generation spheres were used for subsequent assays.

# 2.3 PNA-TPP design, preparation and treatment

PNA-TPP was designed to target the common sequence shared by the light-strand and heavy-strand promoters in the mitochondrial DNA D-loop region. The target sequence was 5'-CANACCGCCAAAAGA-3'. PNAGENE (Korea) constructed and synthesized the PNA-TPP complex. PNA was used to bind this sequence and block mitochondrial DNA transcription. PNA-TPP powder was dissolved in sterile water to make a 1 mM stock solution. It was then diluted with serum-free medium before use. A549 stem cell spheres were collected and allowed to settle. The old medium was removed. Serum-free medium containing PNA-TPP was then added.

## 2.4 Experimental grouping and interventions

A549 cells and A549-derived stem cell spheres were used as the main models. For basic comparison, A549 cells and A549 stem cell spheres were compared to evaluate mitochondrial Drp1 and apoptosis-related protein expression. Based on our previous work and preliminary validation, 10 nmol/mL PNA-TPP was selected as the working concentration in this study [15]. This concentration is equivalent to 10 μM and was used for 24 h treatment in subsequent functional experiments. The PNA-TPP treatment experiment included the Control and PNA-TPP groups. The combined-intervention assay included Control, CDDP, and PNA-TPP + CDDP groups. The CDDP group was treated with 80 μM cisplatin for 24 h. The PNA-TPP + CDDP group received 10 nmol/mL PNA-TPP for 24 h and then 80 μM cisplatin for another 24 h. The Drp1 overexpression experiment included OE-NC and OE-Drp1 groups. The Drp1 overexpression plus cisplatin experiment included OE-NC + CDDP and OE-Drp1 + CDDP groups. For Drp1 knockdown screening, the groups included sh-NC, sh-Drp1-1, sh-Drp1-2, and sh-Drp1-3. The reversal experiment included PNA-TPP + sh-NC and PNA-TPP + sh-Drp1 groups. CDDP was purchased from MCE (Cat. No. HY17394). A stock solution was prepared by dissolving 10 mg cisplatin in 167 μL DMSO to obtain 200 mM, followed by dilution with culture medium. The 80 μM dose was chosen according to reported A549 and A549 sphere treatment ranges and preliminary results. This concentration caused detectable but incomplete inhibition of A549 stem cell spheres. The final DMSO concentration was kept the same among groups and maintained within a non-toxic range.

## 2.5 Drp1 overexpression lentiviral transduction

Drp1 overexpression was achieved by lentiviral transduction. The full-length DNM1L/Drp1 sequence was synthesized and inserted into the pDS087-pL6-TO-V5-GIM lentiviral vector. A matched negative control lentivirus was also prepared. Second-generation A549 stem cell spheres were harvested and counted. Cells were then seeded into 96-well plates at about 4000 cells/well. After 24 h of culture, the lentivirus was diluted in fresh SFM medium at the required MOI. The old medium was removed, and 100 μL diluted virus was added to each well. After 8–12 h, the virus-containing medium was replaced with fresh SFM medium. Fluorescence was checked at 24, 48, and 72 h. Western blotting was used to verify Drp1 overexpression. The cells were then used for assays of mitochondrial function, sphere formation, stemness markers, apoptosis, migration, and invasion.

## 2.6 Drp1 knockdown by shRNA

Drp1 was silenced by shRNA lentiviral transduction. Three shRNA oligos were designed according to the DRP1/DNM1L sequence. The sequences are listed in **Table S1**. These oligos were inserted into the PL/IRES/green fluorescent protein (GFP)/U6 lentiviral interference vector. Three Drp1-targeting shRNA lentiviral constructs were generated and named PL-DNM1L-SH1, PL-DNM1L-SH2, and PL-DNM1L-SH3. In the experimental groups, these constructs were referred to as sh-Drp1-1, sh-Drp1-2, and sh-Drp1-3, respectively. A negative control virus was prepared at the same time. Second-generation A549 stem cell spheres were harvested and counted. Cells were seeded into 96-well plates at about 4000 cells/well. Lentiviral transduction was performed after 24 h. The viral titer was about 1–1.5 × $10^8$ TU/mL. The virus was diluted in fresh SFM medium at the indicated MOI. Then, 100 μL diluted virus was added to each well after medium removal. The plate was gently shaken. After 8–12 h, fresh SFM medium was added to replace the viral solution. GFP fluorescence was checked at 24, 48, and 72 h. Drp1 knockdown was verified by Western blotting and qPCR. According to transduction efficiency and Drp1 reduction, sh-Drp1-2 was chosen for later experiments.

# 2.7 Cell viability assay

Cell viability was detected with a CCK-8 kit from GLPBIO (Cat. No. GK10001). A549 stem cell spheres or treated cells were harvested and made into a cell suspension. Cells were plated in 96-well plates at 6000 cells/well with 100 μL suspension. Each group had three replicate wells. Sterile PBS was added to the outer wells to limit evaporation. After overnight culture at 37°C with 5% $CO_2$, cells received the indicated treatments. Then, 10 μL CCK-8 reagent was added to each well. The plates were kept in the dark for 1–2 h. Absorbance was measured at 450 nm.

# 2.8 Colony formation assay

The colony formation assay was used to evaluate the long-term clonogenic capacity of A549-derived stem-like sphere cells after cisplatin-based treatment or Drp1 overexpression. Briefly, treated cells were collected, digested, centrifuged, and resuspended into a single-cell suspension. After counting, cells were seeded into 6-well plates at 600 cells per well with 3 mL medium. For the combined-treatment experiment, cells were assigned to the Control, CDDP, and PNA-TPP + CDDP groups. For the Drp1 overexpression experiment under cisplatin treatment, cells were assigned to the OE-NC + CDDP and OE-Drp1 + CDDP groups. Cells were cultured at 37°C with 5% $CO_2$ for 2–3 weeks. When visible colonies appeared, the medium was removed. Cells were washed two to three times with PBS, fixed with 1 mL methanol for 15 min, and stained with 1 mL 0.1% crystal violet for 10–30 min. Excess dye was washed off with running water, and the plates were dried. Cell clusters containing at least 50 cells were defined as colonies. Colonies were counted under a microscope and photographed.

# 2.9 Sphere formation assay

The sphere formation assay was used to evaluate self-renewal. After treatment, sphere-forming cells from each group were collected and gently dispersed into a single-cell suspension. The suspension was filtered through a cell strainer and counted. Cells were seeded at the same density into low-attachment 6-well plates and cultured in serum-free sphere-forming medium. Fresh medium was added every 3–5

days according to growth status. After 7–14 days, spheres were observed and imaged under an inverted microscope. Spheres larger than 50 μm or containing more than 50 cells were included. Several random fields were counted for each group.

## 2.10 Apoptosis analysis by flow cytometry

Apoptosis was measured with an Annexin V-FITC/PI Apoptosis Kit (C1062L, Beyotime). After treatment, cells were harvested and centrifuged at 300 × g for 5 min. The cells were washed with PBS, resuspended, and counted. For each sample, 1–5 × $10^5$ cells were collected and washed again. The cells were then suspended in 100 μL diluted 1× Annexin V Binding Buffer. Next, 2.5 μL Annexin V-FITC Reagent and 2.5 μL PI Reagent were added. The mixture was incubated at room temperature in the dark for 15–20 min. After staining, 400 μL diluted 1× Annexin V Binding Buffer was added. Samples were detected immediately using a flow cytometer (RaiseCyte 2L6C, RayCeler). Total apoptosis was calculated as the percentage of Annexin V-positive cells, including early and late apoptotic cells.

## 2.11 Mitochondrial membrane potential assay

Mitochondrial membrane potential was assessed with a JC-1 assay kit (MT09, Dojindo). After treatment, cells were harvested, washed twice with PBS, and centrifuged. A total of 2–5 × $10^5$ cells were used for each sample. The JC-1 working solution was prepared as instructed. First, 100 μL 10× incubation buffer was diluted with 900 μL sterile water and warmed to 37°C. Then, 5 μL JC-1 was mixed with 500 μL 1× incubation buffer. Cells were suspended in 500 μL JC-1 working solution and incubated at 37°C with 5% $CO_2$ for 15 min in the dark. After centrifugation, cells were resuspended in 500 μL preheated 1× incubation buffer. JC-1 red aggregates and green monomers were detected by flow cytometry (RaiseCyte 2L6C, RayCeler). A higher green monomer proportion or a lower red/green fluorescence ratio indicated mitochondrial membrane potential loss.

## 2.12 DCFH-DA flow cytometry and DHE fluorescence staining

Intracellular ROS levels were evaluated using DCFH-DA flow cytometry (Beyotime, Cat. No. S0033S) and DHE fluorescence staining. For flow cytometric analysis, cells were stained with DCFH-DA. After treatment, DCFH-DA was diluted 1:1000 in serum-free medium to a final concentration of 10 μmol/L. The culture medium was removed, and cells were incubated with the DCFH-DA working solution at 37°C for 20 min in the dark. After incubation, cells were washed three times with serum-free medium to remove excess probe. Cells were then digested, harvested, centrifuged at about 200 × g for 3 min, washed with PBS, and resuspended for immediate flow cytometric analysis. ROS levels were quantified using the mean fluorescence intensity (MFI) of DCFH-DA. For fluorescence microscopy, cells were stained with DHE. DHE can cross the cell membrane and is oxidized by intracellular ROS to ethidium-like products, which intercalate into nucleic acids and emit red fluorescence. After staining, cells were observed under a fluorescence microscope. The red fluorescence signal was used to show ROS-related accumulation.

## 2.13 ATP measurement by ELISA

Cellular ATP levels were detected with a human ATP ELISA kit from Enzyme-linked Biotechnology (Cat. No. MM-14432H2). After treatment, cells were harvested and suspended in PBS at pH 7.2–7.4. The samples were lysed by ultrasound and centrifuged at about 500–1000 × g for 20 min at 2–8°C. The supernatant was collected for ELISA. Standard wells received 50 µL standard solution. Sample wells received 40 µL sample diluent and 10 µL sample. The plate was sealed and incubated at 37°C for 30 min. After five washes, 50 µL enzyme-labeled reagent was added. The plate was incubated again at 37°C for 30 min. Then, 50 µL chromogenic reagent A and 50 µL chromogenic reagent B were added after washing. The plate was protected from light at 37°C for 10 min. Finally, 50 µL stop solution was added. Absorbance was read at 450 nm. ATP levels were calculated using the standard curve and adjusted by the dilution factor.

## 2.14 Wound healing and Transwell invasion assays

Cell migration was evaluated by wound healing assay. For the wound healing assay, A549-derived stem-like spheres were collected and gently dissociated into single cells. The cells were then seeded into 6-well plates and cultured under adherent conditions until they reached approximately 90% confluence. A linear wound was made using a sterile 200-µL pipette tip. Detached cells were removed with PBS. Serum-free or low-serum medium was added, and images were taken at 0 h and 24 h under an inverted microscope. The wound area was analyzed using ImageJ software. Cell invasion was tested using Transwell chambers (110304027, BKMANLAB) coated with Matrigel (0827065, Abcam). Matrigel was thawed at 4°C, diluted with basal medium at 2:1, and added to the upper chamber at 20 µL/well. After gel formation at 37°C, 0.3 mL serum-free cell suspension containing $3 \times 10^4$–$10 \times 10^4$ cells/well was placed in the upper chamber. The lower chamber was filled with 0.5 mL complete medium. After incubation, non-invaded cells were removed. Invaded cells were fixed with paraformaldehyde for 15 min and stained with crystal violet for 5 min. The chambers were washed, dried, and imaged under an inverted microscope. Invaded cells were counted in three to five random fields per well.

## 2.15 Quantitative real-time PCR

Drp1 mRNA was measured by RT-qPCR. After treatment, total RNA was isolated with the TransZol Up Plus RNA Kit. Only qualified RNA was used for cDNA synthesis. Genomic DNA was removed first. Reverse transcription was then performed using TransScript® Uni All-in-One First-Strand cDNA Synthesis SuperMix for qPCR. qPCR was conducted with MagicSYBR Mixture in a SYBR Green system. Each 20 µL reaction included 10 µL 2× SYBR qPCR Master Mix, 1 µL cDNA, 0.4 µL forward primer, 0.4 µL reverse primer, and 8.2 µL RNase-free dd$H_2O$. The program was 95°C for 10 min, followed by 40 cycles of 95°C for 10 s, 60°C for 30 s, and 72°C for 30 s. GAPDH served as the reference gene. Sangon Biotech Co., Ltd. (Shanghai, China) synthesized the Drp1 and GAPDH primers. The primer sequences are shown in Table 1. The 2-ΔΔCt method was used to calculate relative Drp1 mRNA expression.

Table 1
Primer sequences used for qPCR

| Gene | Forward primer 5'–3' | Reverse primer 5'–3' |
|---|---|---|
| GAPDH | GTCTCCTCTGACTTCAACAGCG | ACCACCCTGTTGCTGTAGCCAA |
| Drp1 | GATGCCATAGTTGAAGTGGTGAC | CCACAAGCATCAGCAAAGTCTGG |

# 2.16 Mitochondrial protein extraction and Western blot

Mitochondrial proteins were prepared for mitochondrial Drp1 detection. After treatment, cells were harvested, washed with ice-cold PBS, and resuspended in 3 mL ice-cold PBS for counting. Cells were centrifuged at 600 × g for 5 min at 4°C. The pellet was mixed with 1–2.5 mL mitochondrial isolation reagent and kept on ice for 15 min. Cells were then homogenized with 10–30 strokes in a glass homogenizer. Trypan blue staining was used to check cell disruption. When more than 50% of cells were trypan blue-positive, the homogenate was centrifuged at 600 × g for 10 min at 4°C. The supernatant was collected and centrifuged at 11,000 × g for 10 min at 4°C. The mitochondrial pellet was lysed with 100 μL mitochondrial lysis buffer containing PMSF. Total proteins were extracted with RIPA lysis buffer. Protein concentration was measured by the BCA method. Equal amounts of total or mitochondrial proteins were separated by SDS-PAGE and transferred onto PVDF membranes. Membranes were blocked with 5% non-fat milk for 2 h and incubated with primary antibodies overnight at 4°C. After TBST washing, membranes were incubated with HRP-conjugated secondary antibodies for 2 h at room temperature. Bands were detected with ECL reagent and imaged using a gel imaging system. The primary antibodies included anti-Drp1 antibody (Cell Signaling Technology, Cat. No. 8570; 1:1000), anti-OCT4/POU5F1 antibody (Proteintech, Cat. No. 60242-1-Ig; 1:1000), anti-SOX2 antibody (Proteintech, Cat. No. 11064-1-AP; 1:1000), anti-NANOG antibody (Proteintech, Cat. No. 67255-1-Ig; 1:1000), anti-Bcl-2 antibody (Proteintech, Cat. No. 26593-1-AP; 1:1000), anti-Bax antibody (Proteintech, Cat. No. 50599-2-Ig; 1:1000), anti-COX IV antibody (Proteintech, Cat. No. 66110-1-Ig; 1:5000), anti-GAPDH antibody (Proteintech, Cat. No. 60004-1-Ig; 1:50000), and anti-β-actin antibody (Proteintech, Cat. No. 66009-1-Ig; 1:2000). HRP-conjugated goat anti-rabbit IgG (H + L) (HS101-01, TransGen Biotech) and HRP-conjugated goat anti-mouse IgG (H + L) (HS201-01, TransGen Biotech) were used as secondary antibodies at 1:5000.

# 2.17 Statistical analysis

Each experiment was performed at least three independent times. Results are expressed as mean ± SD. GraphPad Prism was used for statistical analysis. Data normality was assessed before choosing the test. For two groups, unpaired Student's t-test was used for normally distributed data. Mann–Whitney U test was used for non-normal data. For three or more groups, one-way ANOVA with Tukey's post hoc test was applied when the data met parametric assumptions. Kruskal–Wallis test was used for non-normal data. Multiple-group analysis was applied to cisplatin co-treatment, Drp1 knockdown screening, and rescue experiments. All tests were two-sided. $P < 0.05$ was considered statistically significant. Figure labels were shown as *$P < 0.05$, **$P < 0.01$, ***$P < 0.001$, and ns for no significance.

# 3 Results

## 3.1 Establishment and characterization of A549-derived stem-like spheres

To establish an A549-derived lung cancer stem-like model, A549 cells were induced to form spheres by single-cell cloning and serum-free suspension culture. Under the microscope, A549 cells formed monoclonal-like clusters (Fig. 1A). In serum-free suspension culture, first-generation stem cell spheres were observed (Fig. 1B). After passage, second-generation spheres were obtained (Fig. 1C). Western blotting showed lower mitochondrial Drp1 expression in A549 stem cell spheres than in parental A549 cells (Fig. 1D). Apoptosis-related protein detection showed higher B-cell lymphoma 2 (Bcl-2) expression and lower BCL2-associated X protein (Bax) expression in A549 stem cell spheres (Fig. 1E). These findings suggest that A549 cells can form a stem-like spheroid cell population. This process was accompanied by changes in mitochondrial Drp1 and apoptosis-related proteins. This model was then used to study the effects of PNA-TPP on Drp1-related mitochondrial function and cisplatin response.

## 3.2 PNA-TPP increases Drp1 expression in A549-derived stem-like spheres

Based on our previous work and preliminary validation, 10 nmol/mL PNA-TPP, equivalent to 10 μM, was used as the working concentration for subsequent experiments. This concentration was selected because it had been used to evaluate mitochondrial localization and mitochondrial functional changes in A549 cells in previous studies. qRT-PCR results showed that Drp1 mRNA expression was increased in A549 stem cell spheres after PNA-TPP treatment compared with the Control group (Fig. 2A). Western blot results showed that Drp1 levels in the mitochondrial protein fraction were also increased after PNA-TPP treatment (Fig. 2B). These results suggest that PNA-TPP treatment can upregulate Drp1 mRNA expression and increase mitochondrial Drp1 protein levels in A549-derived stem-like spheres.

## 3.3 PNA-TPP induces mitochondrial dysfunction and suppresses stem-like phenotypes

After confirming that PNA-TPP affected Drp1 expression, we further evaluated its effects on mitochondrial function-related indicators in A549 lung cancer stem cell spheres. JC-1 flow cytometry showed that the proportion of JC-1 green monomers was increased in the PNA-TPP group compared with the Control group, indicating a decrease in mitochondrial membrane potential (Fig. 3A). DCFH-DA flow cytometry showed an overall rightward shift of the fluorescence peak in the PNA-TPP group. In parallel, DHE fluorescence staining showed stronger ROS-related red fluorescence signals in the PNA-TPP group, further supporting increased intracellular ROS accumulation after PNA-TPP treatment (Fig. 3B). Meanwhile, ATP levels were reduced in the PNA-TPP group (Fig. 3C). The sphere formation assay showed that PNA-TPP treatment reduced the sphere-forming ability of A549 lung cancer stem cell spheres (Fig. 3D). Western blot analysis showed decreased expression of OCT4, SOX2, and NANOG after

PNA-TPP treatment (Fig. 3E). These results suggest that PNA-TPP treatment can induce mitochondrial function-related changes in A549 lung cancer stem cell spheres, including decreased mitochondrial membrane potential, increased ROS levels, and reduced ATP levels, accompanied by a decline in stemness-related phenotypes.

## 3.4 PNA-TPP pretreatment combined with CDDP further suppresses A549-derived spheres

Lung cancer stem-like cells are often linked to cisplatin tolerance. Since the above results showed that PNA-TPP weakened stemness-related phenotypes, we next tested whether PNA-TPP pretreatment could affect the response of A549 lung cancer stem cell spheres to cisplatin. The CCK-8 assay showed that CDDP reduced cell viability, and this reduction was greater in the PNA-TPP + CDDP group (Fig. 4A). Colony formation was also lower after combined treatment than after CDDP treatment alone (Fig. 4B). Flow cytometry showed a higher apoptosis rate in the PNA-TPP + CDDP group than in the CDDP group (Fig. 4C). Western blotting further showed lower B-cell lymphoma 2 expression and higher BCL2-associated X protein expression after combined treatment (Fig. 4D), indicating that PNA-TPP may strengthen CDDP-induced apoptosis. In addition, wound healing and Transwell assays showed that cell migration and invasion were reduced more strongly in the PNA-TPP + CDDP group than in the CDDP group (Fig. 4E, F).

## 3.5 Drp1 overexpression mimics the mitochondrial and stemness-suppressive effects of PNA-TPP

To further examine the involvement of Drp1 in the effects of PNA-TPP, a Drp1 overexpression model was constructed. Western blotting showed that mitochondrial Drp1 levels were increased in the OE-Drp1 group compared with the OE-NC group, confirming effective overexpression (Fig. 5A). Relative to OE-NC cells, OE-Drp1 cells showed a higher proportion of JC-1 green monomers and reduced ATP production. ROS detection showed a rightward shift of the DCFH-DA fluorescence peak and stronger DHE-related red fluorescence signals in the OE-Drp1 group, indicating increased intracellular ROS levels after Drp1 overexpression (Fig. 5B–D). These changes suggest that Drp1 overexpression affects mitochondrial membrane potential, ROS production, and cellular energy metabolism. Sphere formation was also reduced in the OE-Drp1 group (Fig. 5E). Western blotting showed lower OCT4, SOX2, and NANOG levels (Fig. 5F, G). These results indicate that Drp1 overexpression causes mitochondrial changes similar to those induced by PNA-TPP. It is also linked to reduced stemness-related phenotypes.

## 3.6 Drp1 overexpression reduces cisplatin resistance-related phenotypes in A549 lung cancer stem cell spheres

To further examine whether Drp1 overexpression affects the tolerance of A549 lung cancer stem cell spheres to cisplatin, we compared phenotypic changes between the OE-NC and OE-Drp1 groups under cisplatin treatment. Compared with the OE-NC + CDDP group, the OE-Drp1 + CDDP group showed reduced colony formation ability and an increased apoptosis rate (Fig. 6A, B). Western blotting showed

lower Bcl-2 expression and higher BCL2-associated X protein expression in the OE-Drp1 + CDDP group. This suggests that Drp1 overexpression may strengthen the apoptotic response induced by cisplatin (Fig. 6C). In addition, cell migration and invasion were both reduced in the OE-Drp1 + CDDP group compared with the OE-NC + CDDP group (Fig. 6D, E). These results suggest that Drp1 overexpression may reduce cisplatin resistance-related phenotypes in A549 lung cancer stem cell spheres under cisplatin treatment.

## 3.7 Drp1 knockdown partially restores mitochondrial membrane potential and stem-like phenotypes after PNA-TPP treatment

qRT-PCR and Western blotting showed that sh-Drp1-2 reduced Drp1 expression at the mRNA level and in the mitochondrial protein fraction. Thus, sh-Drp1-2 was used in later experiments (Fig. 7A). Under PNA-TPP treatment, JC-1 flow cytometry showed fewer JC-1 green monomers in the PNA-TPP + sh-Drp1 group than in the PNA-TPP + sh-NC group. This indicates a partial recovery of mitochondrial membrane potential (Fig. 7B). The sphere formation assay showed stronger sphere-forming ability in the PNA-TPP + sh-Drp1 group (Fig. 7C). Western blotting also showed increased OCT4, SOX2, and NANOG expression after Drp1 knockdown (Fig. 7D). These findings suggest that Drp1 knockdown partly reverses the decrease in mitochondrial membrane potential caused by PNA-TPP. It may also partly restore sphere formation and stemness-related protein expression in A549 stem cell spheres.

# 4 Discussion

Lung adenocarcinoma remains an important pathological type of non-small cell lung cancer, and cisplatin tolerance is still a key factor affecting treatment efficacy. Our previous study showed that A549 tumor spheres had higher mitochondrial activity and stronger drug-resistant features, and that PNA-mito could interfere with mitochondrial gene expression and enhance the cytotoxic effect of cisplatin on A549 tumor spheres [15]. Based on these findings, the present study further focused on Drp1-related changes in mitochondrial function. The results suggest that mitochondrial dysfunction associated with Drp1 changes may participate in the process by which PNA-TPP weakens the stem cell-like phenotype of A549 cells and reduces cisplatin resistance-related phenotypes.

This study suggests that PNA-TPP may increase the susceptibility of A549 stem cell spheres to stress-related damage by disturbing their mitochondrial metabolic state. After PNA-TPP treatment, ATP levels declined, ROS levels increased, and mitochondrial membrane potential was reduced, indicating impairment of mitochondrial energy production and redox balance. Previous studies reported that cisplatin resistance in NSCLC may involve ROS- and PGC-1α-mediated metabolic reprogramming, and that blocking oxidative phosphorylation can attenuate the resistant phenotype [16]. In addition, inhibiting mitochondrial-encoded proteins, mitochondrial respiration, and membrane potential has been reported to reduce A549 cell survival and promote apoptosis induced by antitumor drugs [17]. These reports support the decrease in ATP production and mitochondrial membrane potential observed after PNA-TPP

treatment in the present study. Other studies have shown that the mitochondrial citrate transporter SLC25A1 contributes to stemness and treatment tolerance in NSCLC cells, suggesting a close association between mitochondrial metabolic regulation and lung cancer stem-like properties [18]. Research on A549 tumor spheres also indicated that lipid synthesis may enhance mitochondrial fusion and help maintain cancer stem cell-like characteristics [19]. Moreover, our previous work showed that A549-derived tumor spheres expressed stemness markers, including CD44, CD133, SOX2, and OCT4, and exhibited stronger drug-resistant features [20]. Therefore, the reduced sphere-forming capacity and lower OCT4, SOX2, and NANOG expression after PNA-TPP treatment may be linked to disturbed mitochondrial metabolism and mitochondrial dynamic homeostasis.

Based on these findings, this study further found that PNA-TPP combined with cisplatin further reduced cell viability, colony formation, migration, and invasion in A549 stem cell spheres and increased apoptosis. Compared with the CDDP group, the reduced B-cell lymphoma 2 expression and increased Bax expression in the PNA-TPP + CDDP group suggest that PNA-TPP may enhance cisplatin-induced mitochondrial apoptosis. Previous studies have reported that miR-204 can restore the sensitivity of cisplatin-resistant NSCLC cells to cisplatin-induced mitochondrial apoptosis by targeting the CAV-1/AKT/Bad pathway [21]. Another study showed that blockade of Bax/Bak-related mitochondrial apoptosis can affect the response of NSCLC cells to therapeutic stimulation, suggesting that restoration of mitochondrial apoptotic capacity may help improve treatment sensitivity [5, 22]. Therefore, the stronger inhibitory effect produced by PNA-TPP combined with cisplatin may be related to the effects of PNA-TPP on mitochondrial homeostasis and stemness maintenance. However, because this study did not systematically distinguish the effect of PNA-TPP alone from the combined-treatment effect in the combination experiments, the possibility of additive cytotoxicity cannot be fully excluded.

Drp1, an important regulator of mitochondrial fission, may be one of the key factors involved in PNA-TPP-induced mitochondrial dysfunction. Abnormal Drp1 activation can affect mitochondrial morphology, oxidative metabolism, and cell death responses. Previous studies have shown that mdivi-1-mediated interference with Drp1-related mitochondrial dynamics can reduce oxidative metabolism and inhibit tumor cell proliferation [23, 24]. However, the role of Drp1 in tumor cells is not fixed and may vary depending on tumor origin, cellular metabolic status, and external stimulation. In lung cancer stem cell research, FIS1 can enhance lung cancer stem cell-like features by promoting mitochondrial fission and mitophagy, suggesting that mitochondrial fission programs are closely related to the regulation of lung cancer stemness [25]. However, when mitochondria are under strong stress, excessive fission may also promote ROS accumulation, mitochondrial membrane potential loss, and apoptosis [26]. In this study, mitochondrial Drp1 levels were increased in A549 stem cell spheres after PNA-TPP treatment. Drp1 overexpression further produced changes similar to those induced by PNA-TPP. These changes included reduced mitochondrial membrane potential, higher ROS levels, lower ATP levels, and decreased expression of stemness-related proteins. More importantly, under cisplatin treatment, Drp1 overexpression also reduced colony formation, migration, and invasion of A549 stem cell spheres and increased apoptosis, suggesting that Drp1 upregulation may reduce cisplatin tolerance in A549 stem cell spheres. These results indicate that Drp1 upregulation is not merely an accompanying phenomenon, but

may participate in PNA-TPP-induced mitochondrial stress, stemness inhibition, and reduced cisplatin tolerance. Based on this, Drp1-related changes in mitochondrial dynamics may contribute to the disruption of mitochondrial homeostasis in A549 stem cell spheres, shifting cells from a relatively tolerant state toward a stress-injury state and thereby making them more susceptible to cisplatin-mediated inhibition.

Finally, the Drp1 knockdown experiment further supported the involvement of Drp1 in the effects of PNA-TPP. After Drp1 knockdown under PNA-TPP treatment, mitochondrial membrane potential was partially restored, and sphere-forming ability and OCT4, SOX2, and NANOG expression also increased. Recent studies suggest that DRP1-related mitochondrial dynamics and mitochondrial remodeling can influence cancer stemness programs and therapy-resistant phenotypes [24, 26]. However, Drp1 knockdown produced only partial reversal, indicating that PNA-TPP may also affect other mitochondrial-related processes, such as mitochondrial DNA transcription, oxidative phosphorylation protein expression, fusion-related proteins, or other metabolic stress pathways. In addition, the acquisition of tumor cell stemness can be accompanied by coordinated changes in pluripotency factors and regulators of mitochondrial biogenesis, suggesting that stemness maintenance is not determined by a single mitochondrial dynamics molecule [27]. Therefore, Drp1-related changes in mitochondrial dynamics are more likely an important component of the PNA-TPP response network rather than the only mechanism.

This study still has several limitations. First, this study was mainly based on A549-derived stem cell-like spheres, and the mechanism has not yet been validated in more lung adenocarcinoma cell lines, cisplatin-resistant cell lines, primary tumor spheres, or in vivo models. Second, although mitochondrial membrane potential, ROS, and ATP levels were detected, mitochondrial functional changes were not systematically evaluated by mitochondrial morphology imaging, oxygen consumption rate, glycolytic flux, mitochondrial DNA transcription profiling, or mitochondrial respiratory chain protein detection. Third, this study mainly measured Drp1 levels in mitochondrial protein fractions, but did not further detect total Drp1, cytoplasmic Drp1, Drp1 phosphorylation sites, or Drp1 mitochondrial translocation. Therefore, it cannot directly prove that PNA-TPP promotes Drp1-mediated mitochondrial fission. Fourth, although Drp1 overexpression and knockdown experiments support the involvement of Drp1 in the effects of PNA-TPP, Drp1 knockdown only produced partial reversal, suggesting that PNA-TPP may also affect mitochondrial DNA transcription, oxidative phosphorylation protein expression, fusion-related proteins, or other metabolic stress pathways. Finally, this study did not systematically evaluate the effects of PNA-TPP on normal lung epithelial cells or non-tumor cells, so its selectivity and safety still require further validation.

In summary, this study shows that PNA-TPP may induce Drp1-related mitochondrial dysfunction in A549 lung adenocarcinoma stem-like cells. This was reflected by lower mitochondrial membrane potential, higher ROS levels, and reduced ATP production. These mitochondrial changes were accompanied by weaker sphere-forming ability and decreased expression of stemness-related proteins. PNA-TPP also enhanced the inhibitory effect of a fixed concentration of cisplatin on A549 stem cell spheres. Drp1 overexpression partly mimicked the mitochondrial injury and stemness-inhibitory phenotypes induced by

PNA-TPP, while Drp1 knockdown partially restored mitochondrial membrane potential and stemness-related phenotypes after PNA-TPP treatment. These results suggest that Drp1-related mitochondrial functional changes may participate in the process by which PNA-TPP reduces cisplatin tolerance in A549 lung adenocarcinoma stem cell-like cells. However, the specific causal mechanism still needs to be further verified through studies of Drp1 translocation, phosphorylation, mitochondrial morphology, and in vivo experiments.

# Abbreviations

ATP
adenosine triphosphate
Bax
BCL2-associated X protein
Bcl-2
B-cell lymphoma 2
bFGF/FGF-2
basic fibroblast growth factor/fibroblast growth factor 2
CDDP
cisplatin
COX IV
cytochrome c oxidase subunit IV
CSCs
cancer stem cells
DNM1L
dynamin 1-like protein
Drp1
dynamin-related protein 1
EGF
epidermal growth factor
GFP
green fluorescent protein
JC-1
5,5',6,6'-tetrachloro-1,1',3,3'-tetraethylbenzimidazolylcarbocyanine iodide
MFI
mean fluorescence intensity
NANOG
Nanog homeobox
NSCLC
non-small cell lung cancer
OCT4/POU5F1

octamer-binding transcription factor 4/POU class 5 homeobox 1
PNA
peptide nucleic acid
PNA-TPP
peptide nucleic acid conjugated with triphenylphosphonium
ROS
reactive oxygen species
SOX2
SRY-box transcription factor 2

# Declarations

Conflict of Interest Statement

The authors have no conflicts of interest to declare.

Funding Sources

Jiangxi Provincial Health Commission Science and Technology Plan Project (NO. 202210500)

Data Availability Statement

All data generated or analyzed during this study are included in this published article and its supplementary information files. Additional raw data supporting the findings of this study are available from the corresponding author upon reasonable request.

Ethics Approval

This study did not involve human participants, human tissue samples, or animal experiments; therefore, ethical approval was not required.

Author Contributions

Lixia Xie: Conceptualization, Methodology, Investigation, Funding acquisition, Writing – original draft. Yong Cheng: Methodology, Investigation, Data curation, Writing – original draft. Guofeng Zhu: Investigation, Formal analysis, Visualization. Xinyi Zhang: Data curation, Software, Validation. Xiaoqun Ye: Supervision, Writing – review and editing. All authors read and approved the final manuscript.

# References

1. Bray F, Laversanne M, Sung H, Ferlay J, Siegel RL, Soerjomataram I, et al. Global cancer statistics 2022: GLOBOCAN estimates of incidence and mortality worldwide for 36 cancers in 185 countries. CA Cancer J Clin. 2024;74(3):229–63. 10.3322/caac.21834.

2. Kratzer TB, Bandi P, Freedman ND, Smith RA, Travis WD, Jemal A, et al. Lung cancer statistics, 2023. Cancer. 2024;130(8):1330–48. 10.1002/cncr.35128.
3. Sung H, Ferlay J, Siegel RL, Laversanne M, Soerjomataram I, Jemal A, et al. Global Cancer Statistics 2020: GLOBOCAN Estimates of Incidence and Mortality Worldwide for 36 Cancers in 185 Countries. CA Cancer J Clin. 2021;71(3):209–49. 10.3322/caac.21660.
4. Zhang Y, Vaccarella S, Morgan E, Li M, Etxeberria J, Chokunonga E, et al. Global variations in lung cancer incidence by histological subtype in 2020: a population-based study. Lancet Oncol. 2023;24(11):1206–18. 10.1016/S1470-2045(23)00444-8.
5. Liu YT, Cai HR, Li H, Mu QR, Huang JY, Gao Y. Buzhong yiqi decoction improves cisplatin resistance in non-small cell lung cancer by inhibiting PCBP1 to activate the ferritinophagy-mediated ferroptosis pathway. J Ethnopharmacol. 2025;353(Pt A):120317. 10.1016/j.jep.2025.120317.
6. Song Y, Wang L, Zheng Y, Jia L, Li C, Chao K, et al. Deubiquitinating enzyme USP28 inhibitor AZ1 alone and in combination with cisplatin for the treatment of non-small cell lung cancer. Apoptosis. 2024;29(9–10):1793–809. 10.1007/s10495-024-02008-6.
7. Xie M, Yang Z, Zhou J, Chen X, Pu L, Xiong G, et al. ACTG1 mediates cisplatin resistance in NSCLC through induction of mitochondrial fragmentation. Apoptosis. 2025;30(11–12):3069–86. 10.1007/s10495-025-02177-y.
8. Sarin N, Engel F, Kalayda GV, Mannewitz M, Cinatl J Jr., Rothweiler F, et al. Cisplatin resistance in non-small cell lung cancer cells is associated with an abrogation of cisplatin-induced G2/M cell cycle arrest. PLoS ONE. 2017;12(7):e0181081. 10.1371/journal.pone.0181081.
9. Wang L, Liu X, Ren Y, Zhang J, Chen J, Zhou W, et al. Cisplatin-enriching cancer stem cells confer multidrug resistance in non-small cell lung cancer via enhancing TRIB1/HDAC activity. Cell Death Dis. 2017;8(4):e2746. 10.1038/cddis.2016.409.
10. Mao X, Lee NK, Saad SE, Fong IL. Clinical translation for targeting DNA damage repair in non-small cell lung cancer: a review. Transl Lung Cancer Res. 2024;13(2):375–97. 10.21037/tlcr-23-742.
11. Huang W, Sun W, Yang Z, Li Y, Wang Z. Mitochondrial dynamics in cisplatin resistance: molecular mechanisms and therapeutic targeting. Front Oncol. 2025;15:1736487. 10.3389/fonc.2025.1736487.
12. Wang Y, Wang Y, Liu W, Ding L, Zhang X, Wang B, et al. TIM-4 orchestrates mitochondrial homeostasis to promote lung cancer progression via ANXA2/PI3K/AKT/OPA1 axis. Cell Death Dis. 2023;14(2):141. 10.1038/s41419-023-05678-3.
13. Horibe S, Ishikawa K, Nakada K, Wake M, Takeda N, Tanaka T, et al. Mitochondrial DNA mutations are involved in the acquisition of cisplatin resistance in human lung cancer A549 cells. Oncol Rep. 2022;47(2). 10.3892/or.2021.8243.
14. Wang N, Wang X, Lan B, Gao Y, Cai Y. DRP1, fission and apoptosis. Cell Death Discov. 2025;11(1):150. 10.1038/s41420-025-02458-0.
15. Chen SS, Tu XY, Xie LX, Xiong LP, Song J, Ye XQ. Peptide nucleic acids targeting mitochondria enhances sensitivity of lung cancer cells to chemotherapy. Am J Transl Res. 2018;10(9):2940–8.

16. Cruz-Bermudez A, Laza-Briviesca R, Vicente-Blanco RJ, Garcia-Grande A, Coronado MJ, Laine-Menendez S, et al. Cisplatin resistance involves a metabolic reprogramming through ROS and PGC-1alpha in NSCLC which can be overcome by OXPHOS inhibition. Free Radic Biol Med. 2019;135:167–81. 10.1016/j.freeradbiomed.2019.03.009.
17. Dijk SN, Protasoni M, Elpidorou M, Kroon AM, Taanman JW. Mitochondria as target to inhibit proliferation and induce apoptosis of cancer cells: the effects of doxycycline and gemcitabine. Sci Rep. 2020;10(1):4363. 10.1038/s41598-020-61381-9.
18. Fernandez HR, Gadre SM, Tan M, Graham GT, Mosaoa R, Ongkeko MS, et al. The mitochondrial citrate carrier, SLC25A1, drives stemness and therapy resistance in non-small cell lung cancer. Cell Death Differ. 2018;25(7):1239–58. 10.1038/s41418-018-0101-z.
19. Liu Z, Lei J, Wu T, Hu W, Zheng M, Wang Y, et al. Lipogenesis promotes mitochondrial fusion and maintains cancer stemness in human NSCLC. JCI Insight. 2023;8(6). 10.1172/jci.insight.158429.
20. Sun FF, Hu YH, Xiong LP, Tu XY, Zhao JH, Chen SS, et al. Enhanced expression of stem cell markers and drug resistance in sphere-forming non-small cell lung cancer cells. Int J Clin Exp Pathol. 2015;8(6):6287–300.
21. Huang G, Lou T, Pan J, Ye Z, Yin Z, Li L, et al. MiR-204 reduces cisplatin resistance in non-small cell lung cancer through suppression of the caveolin-1/AKT/Bad pathway. Aging. 2019;11(7):2138–50. 10.18632/aging.101907.
22. Li J, Gao G, Ouyang W, Huang J, Liu H, Li J. A rhodamine-coordinated iridium complex to overcome cisplatin-resistant cancer via regulating mitochondrial function triggered apoptosis and ferroptosis. Redox Biol. 2025;81:103536. 10.1016/j.redox.2025.103536.
23. Dai W, Wang G, Chwa J, Oh ME, Abeywardana T, Yang Y, et al. Mitochondrial division inhibitor (mdivi-1) decreases oxidative metabolism in cancer. Br J Cancer. 2020;122(9):1288–97. 10.1038/s41416-020-0778-x.
24. Wang Z, Tang S, Cai L, Wang Q, Pan D, Dong Y, et al. DRP1 inhibition-mediated mitochondrial elongation abolishes cancer stemness, enhances glutaminolysis, and drives ferroptosis in oral squamous cell carcinoma. Br J Cancer. 2024;130(11):1744–57. 10.1038/s41416-024-02670-2.
25. Liu D, Sun Z, Ye T, Li J, Zeng B, Zhao Q, et al. The mitochondrial fission factor FIS1 promotes stemness of human lung cancer stem cells via mitophagy. FEBS Open Bio. 2021;11(7):1997–2007. 10.1002/2211-5463.13207.
26. Giannitti G, Marchesi S, Garavaglia R, Preosto I, Fontana F. Unraveling the role of mitochondrial dynamics in cancer stem cells: Molecular basis and therapeutic implications. Biochim Biophys Acta Rev Cancer. 2025;1880(6):189450. 10.1016/j.bbcan.2025.189450.
27. He B, Gao R, Lv S, Chen A, Huang J, Wang L, et al. Cancer cell employs a microenvironmental neural signal trans-activating nucleus-mitochondria coordination to acquire stemness. Signal Transduct Target Ther. 2023;8(1):275. 10.1038/s41392-023-01487-4.

# Figures

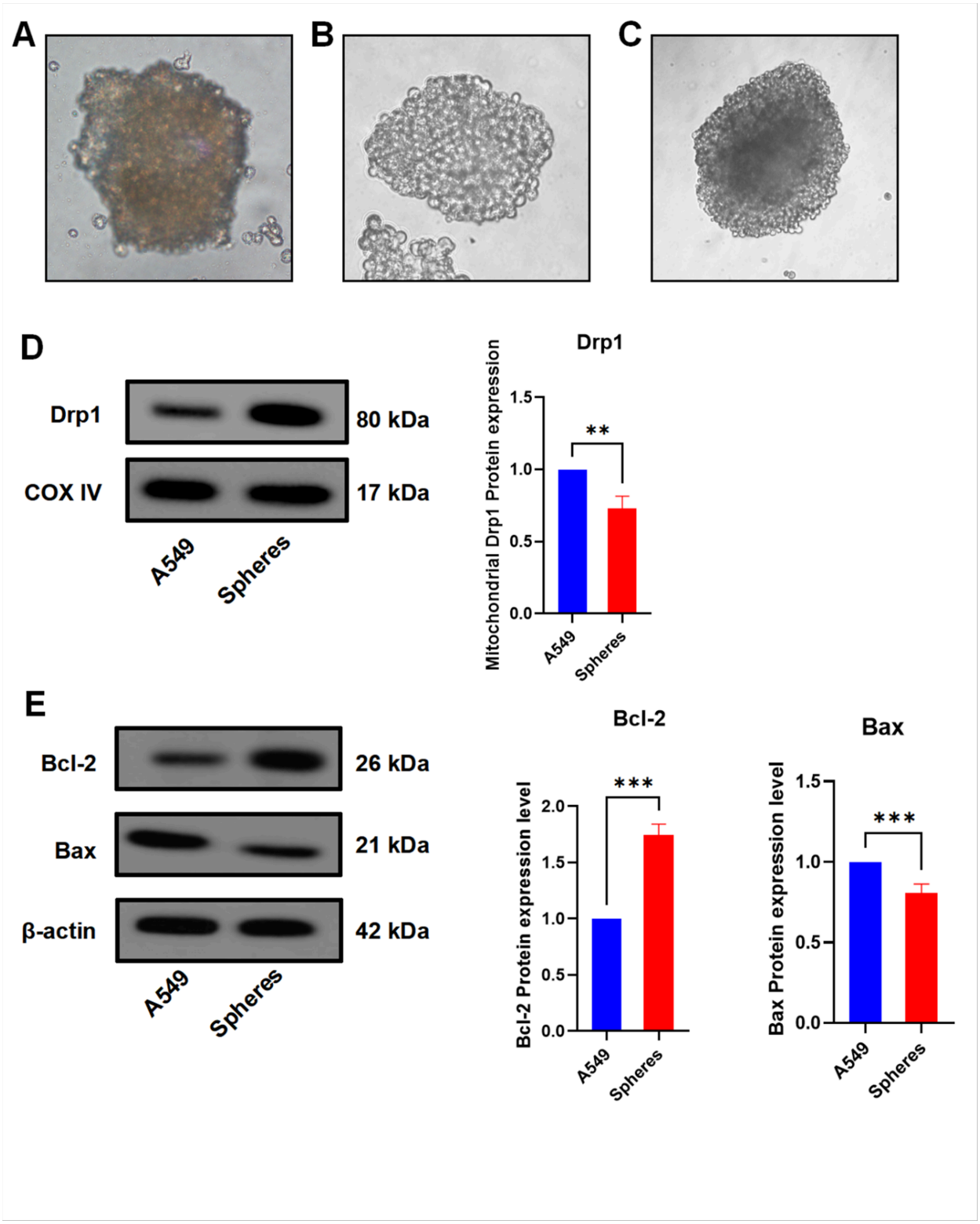



**Figure 1**

Establishment and characterization of A549-derived lung cancer stem cell spheres. (A) Representative images showing monoclonal-like cell clusters formed by A549 cells. Original magnification, 400×. (B) Representative images of first-generation A549 stem cell spheres induced under serum-free suspension culture conditions. Original magnification, 400×. (C) Representative images of second-generation A549 stem cell spheres after passage. Original magnification, 400×. (D) Western blot analysis of Drp1

expression in the mitochondrial protein fraction of parental A549 cells and A549 stem cell spheres. COX IV was used as the mitochondrial loading control. (E) Western blot analysis of apoptosis-related proteins Bcl-2 and Bax in parental A549 cells and A549 stem cell spheres. β-actin was used as the loading control. Data are presented as the mean ± SD from at least three independent experiments. *P < 0.05, **P < 0.01, ***P < 0.001; ns, not significant.

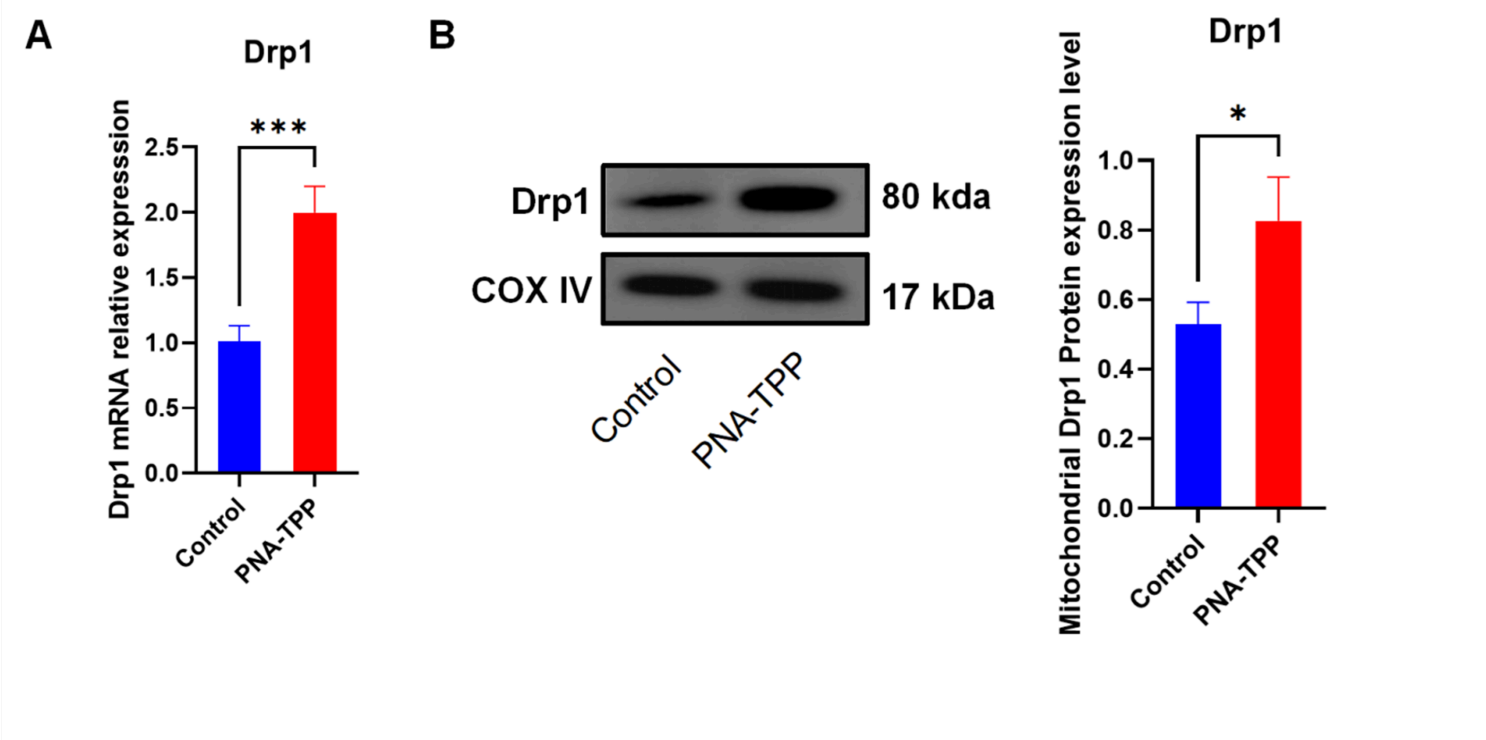
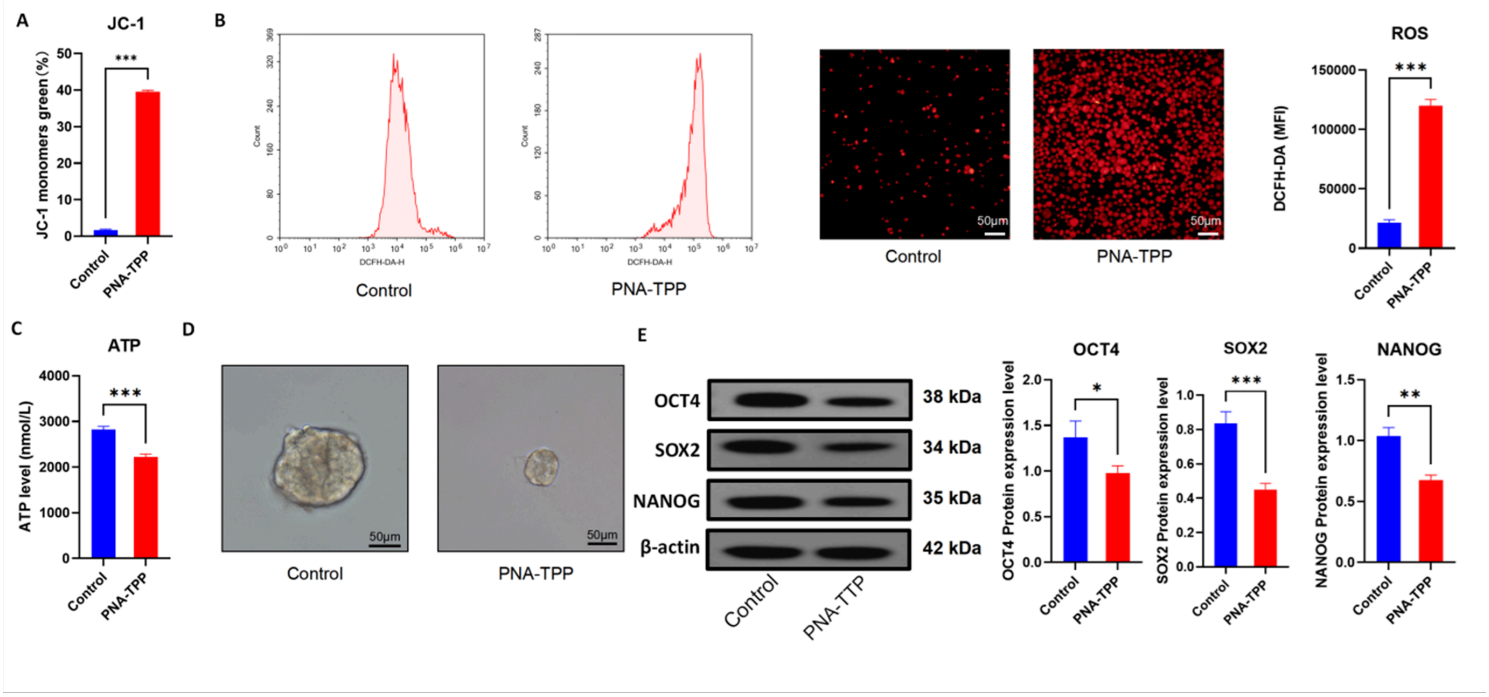


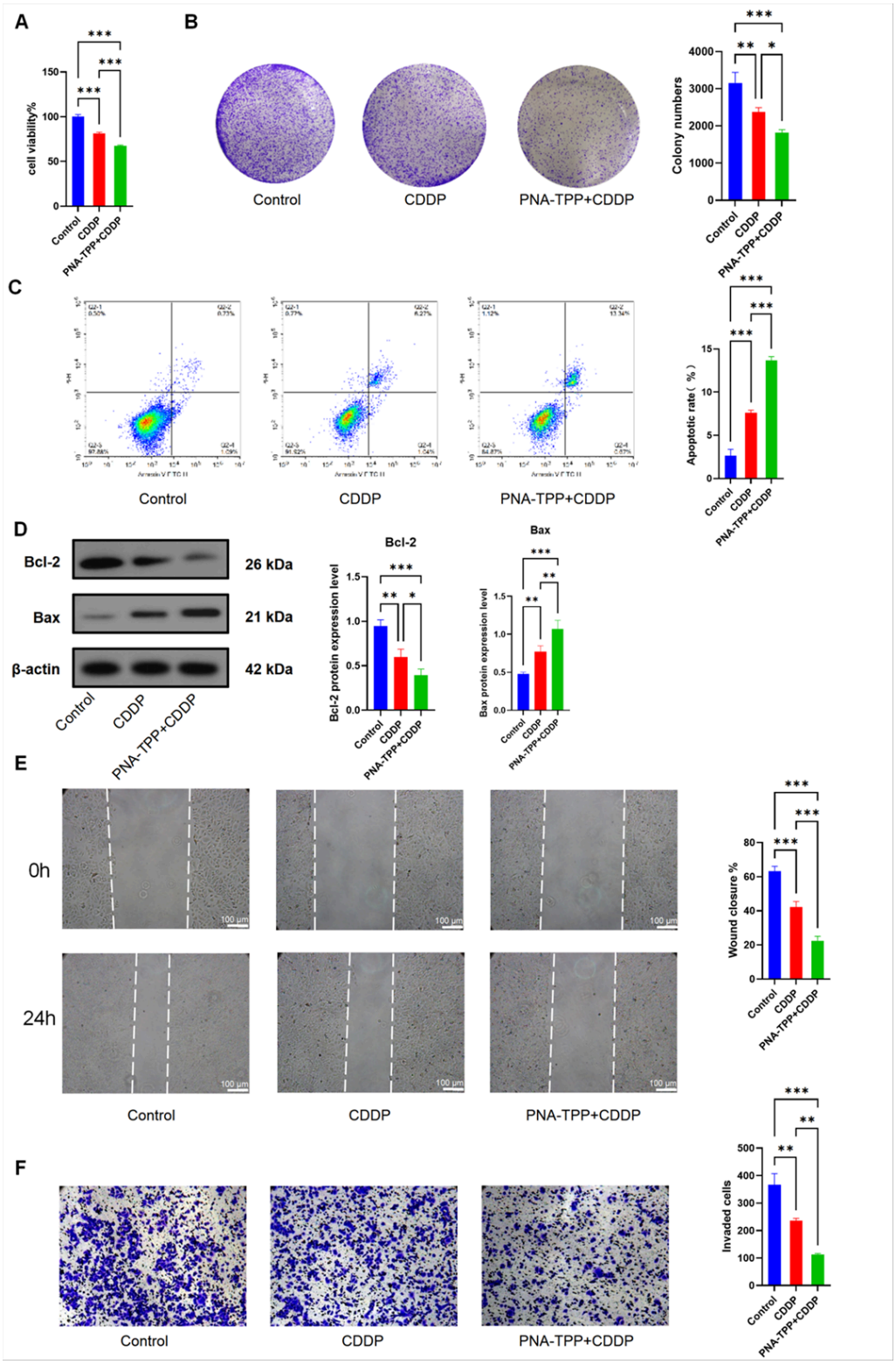

**Figure 2**

Effect of PNA-TPP on Drp1 expression in A549 stem cell spheres. (A) qRT-PCR analysis of Drp1 mRNA expression in A549 stem cell spheres after treatment with 10 nmol/mL PNA-TPP for 24 h. GAPDH was used as the internal reference gene. (B) Western blot analysis of Drp1 expression in the mitochondrial protein fraction after PNA-TPP treatment. COX IV was used as the mitochondrial loading control. Data are presented as the mean ± SD from at least three independent experiments. *P < 0.05, **P < 0.01, ***P < 0.001; ns, not significant.




## Figure 3

Effects of PNA-TPP on mitochondrial function and stemness-related phenotypes in A549 lung cancer stem cell spheres. (A) JC-1 staining combined with flow cytometry was used to detect mitochondrial membrane potential in Control and PNA-TPP-treated A549 stem cell spheres. (B) Intracellular ROS levels were detected using DCFH-DA flow cytometry and DHE fluorescence staining. Scale bar = 50 μm. (C) Cellular ATP levels were measured using an ATP ELISA kit. (D) Sphere formation assay was used to evaluate the sphere-forming ability of A549 stem cell spheres after PNA-TPP treatment. Scale bar = 50 μm. (E) Western blot analysis of stemness-related proteins OCT4, SOX2, and NANOG after PNA-TPP treatment. β-actin was used as the loading control. Data are presented as the mean ± SD from at least three independent experiments. *P < 0.05, **P < 0.01, ***P < 0.001; ns, not significant.




## Figure 4

Effects of PNA-TPP pretreatment combined with cisplatin on A549 lung cancer stem cell spheres. (A) CCK-8 assay was used to detect cell viability in the Control, CDDP, and PNA-TPP + CDDP groups. (B) Colony formation assay was used to evaluate clonogenic ability after different treatments. (C) Annexin V-FITC/PI staining combined with flow cytometry was used to detect cell apoptosis. (D) Western blot analysis of apoptosis-related proteins Bcl-2 and Bax in each group. β-actin was used as the loading

control. (E) Wound healing assay was used to assess cell migration ability. Scale bar = 100 μm. (F) Transwell invasion assay was used to assess cell invasion ability. Scale bar = 100 μm. Data are presented as the mean ± SD from at least three independent experiments. *P < 0.05, **P < 0.01, ***P < 0.001; ns, not significant.

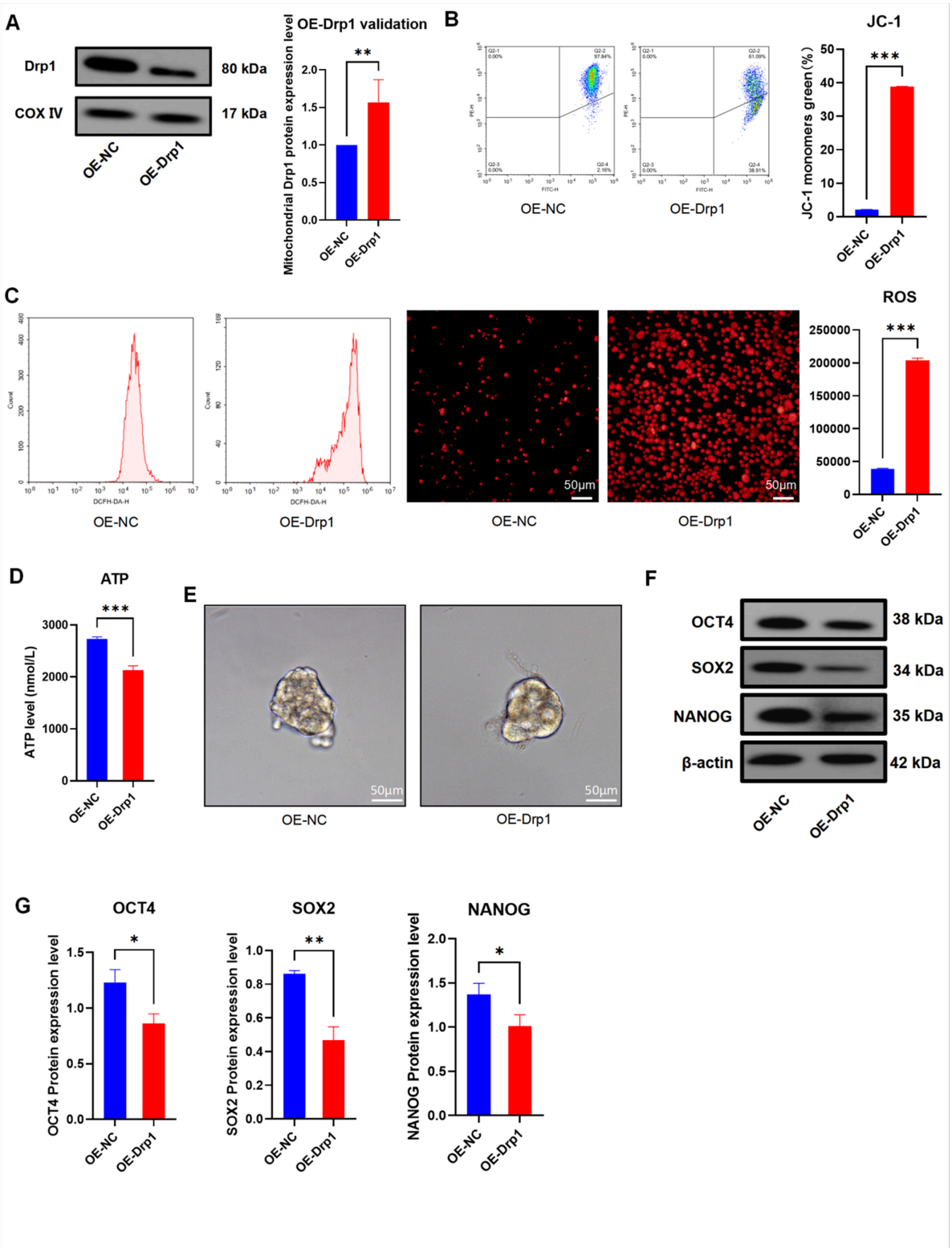



**Figure 5**

Effects of Drp1 overexpression on mitochondrial function and stemness-related phenotypes in A549 lung cancer stem cell spheres. (A) Western blot analysis of Drp1 expression in the mitochondrial protein fraction after lentivirus-mediated Drp1 overexpression. COX IV was used as the mitochondrial loading control. (B) JC-1 staining combined with flow cytometry was used to detect mitochondrial membrane potential in the OE-NC and OE-Drp1 groups. (C) Intracellular ROS levels were detected using DCFH-DA flow cytometry and DHE fluorescence staining. Scale bar = 50 μm. (D) Cellular ATP levels were measured using an ATP ELISA kit. (E) Sphere formation assay was used to evaluate the sphere-forming ability of A549 stem cell spheres after Drp1 overexpression. Scale bar = 50 μm. (F) Western blot analysis of stemness-related proteins OCT4, SOX2, and NANOG. (G) Quantitative analysis of OCT4, SOX2, and NANOG protein expression. β-actin was used as the loading control for total protein analysis. Data are presented as the mean ± SD from at least three independent experiments. *P < 0.05, **P < 0.01, ***P < 0.001; ns, not significant.

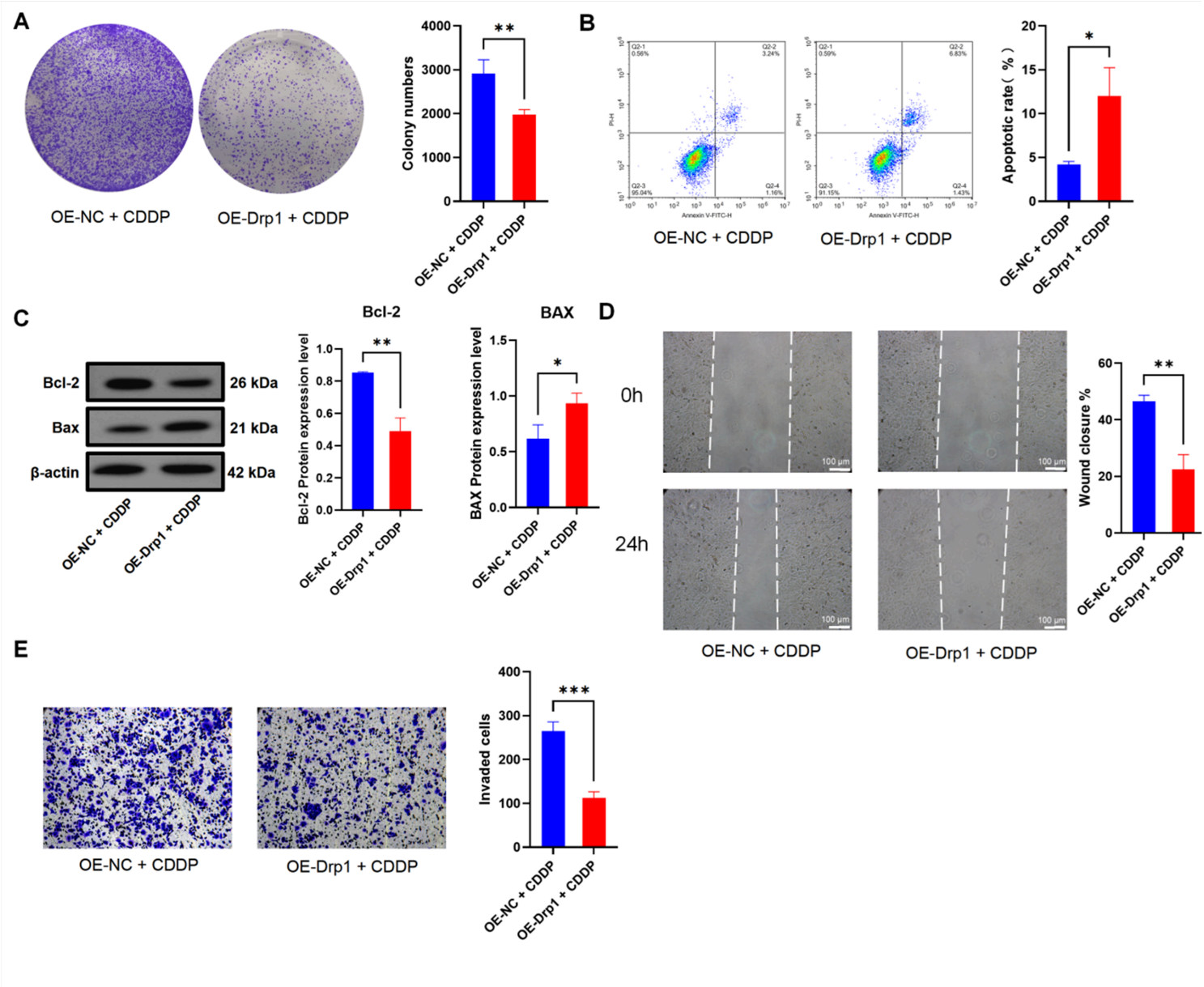
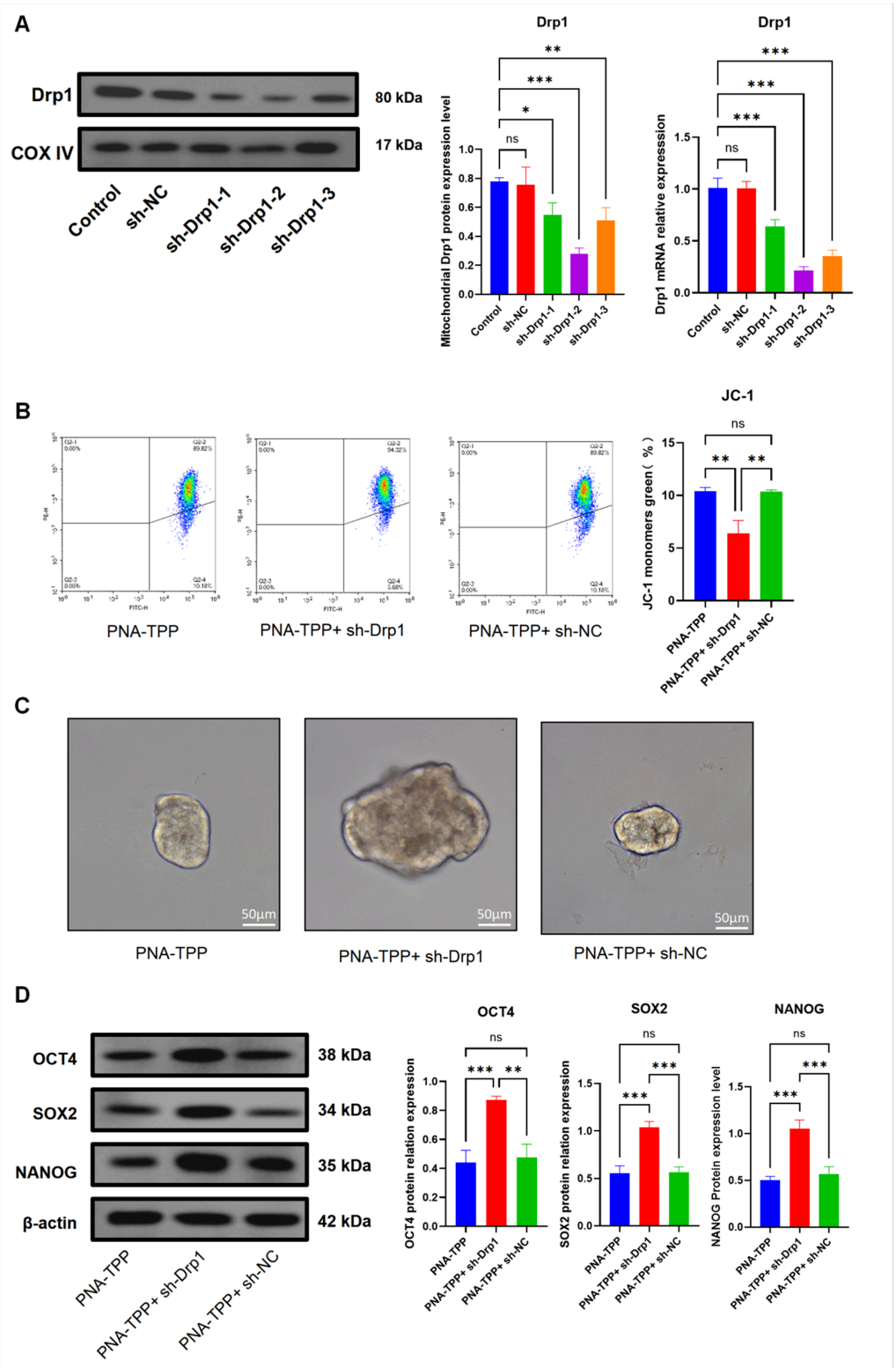



**Figure 6**

Effects of Drp1 overexpression on cisplatin resistance-related phenotypes in A549 lung cancer stem cell spheres. (A) Colony formation assay was used to evaluate clonogenic ability in the OE-NC + CDDP and OE-Drp1 + CDDP groups. (B) Annexin V-FITC/PI staining combined with flow cytometry was used to detect cell apoptosis under cisplatin treatment. (C) Western blot analysis of apoptosis-related proteins Bcl-2 and Bax in each group. β-actin was used as the loading control. (D) Wound healing assay was used to assess cell migration ability under cisplatin treatment. Scale bar = 100 μm. (E) Transwell invasion assay was used to assess cell invasion ability under cisplatin treatment. Scale bar = 100 μm. Data are presented as the mean ± SD from at least three independent experiments. *P < 0.05, **P < 0.01, ***P < 0.001; ns, not significant.




## Figure 7

Drp1 knockdown partially reverses PNA-TPP-induced changes in mitochondrial membrane potential and stemness-related phenotypes. (A) Western blot and qRT-PCR analyses of Drp1 expression after transduction with sh-NC, sh-Drp1-1, sh-Drp1-2, or sh-Drp1-3. COX IV was used as the mitochondrial loading control, and GAPDH was used as the internal reference gene. (B) JC-1 staining combined with flow cytometry was used to detect mitochondrial membrane potential in the PNA-TPP + sh-NC and PNA-

TPP + sh-Drp1 groups. (C) Sphere formation assay was used to evaluate the sphere-forming ability of A549 stem cell spheres after Drp1 knockdown under PNA-TPP treatment. Scale bar = 50 μm. (D) Western blot analysis of stemness-related proteins OCT4, SOX2, and NANOG in the PNA-TPP + sh-NC and PNA-TPP + sh-Drp1 groups. β-actin was used as the loading control. Data are presented as the mean ± SD from at least three independent experiments. *P < 0.05, **P < 0.01, ***P < 0.001; ns, not significant.

## Supplementary Files

This is a list of supplementary files associated with this preprint. Click to download.

- SupplementaryTableS11.docx
- ORIGINALIMAGEWBFORCHECKING.pdf